



**HAL**  
open science

# Fluorinated Zirconia Prepared by Anionic Exchange of Zirconium Oxo/Hydroxide with Trifluoroacetic Acid: Structure, Acid-Base and Catalytic Properties

R. Ben Salem, T. Cornier, P. Bargiela, Bénédicte Lebeau, S. Mishra, N. Essayem

► **To cite this version:**

R. Ben Salem, T. Cornier, P. Bargiela, Bénédicte Lebeau, S. Mishra, et al.. Fluorinated Zirconia Prepared by Anionic Exchange of Zirconium Oxo/Hydroxide with Trifluoroacetic Acid: Structure, Acid-Base and Catalytic Properties. *ChemCatChem*, 2023, 15 (14), pp.e202300169. 10.1002/cctc.202300169 . hal-04108179

**HAL Id: hal-04108179**

**<https://hal.science/hal-04108179>**

Submitted on 8 Sep 2023

**HAL** is a multi-disciplinary open access archive for the deposit and dissemination of scientific research documents, whether they are published or not. The documents may come from teaching and research institutions in France or abroad, or from public or private research centers.

L'archive ouverte pluridisciplinaire **HAL**, est destinée au dépôt et à la diffusion de documents scientifiques de niveau recherche, publiés ou non, émanant des établissements d'enseignement et de recherche français ou étrangers, des laboratoires publics ou privés.



Distributed under a Creative Commons Attribution 4.0 International License

# Fluorinated Zirconia Prepared by Anionic Exchange of Zirconium Oxo/Hydroxide with Trifluoroacetic Acid: Structure, Acid-Base and Catalytic Properties

Roua ben Salem<sup>[a]</sup>, Thibaut Cornier<sup>[a]</sup>, Pascal Bargiela<sup>[a]</sup>, Bénédicte Lebeau<sup>[b][c]</sup>, Shashank Mishra<sup>[a]\*</sup>, and Nadine Essayem<sup>[a]</sup> \*

[a] R. Ben Salem, T. Cornier, P. Bargiela, Dr S. Mishra, Dr N. Essayem  
Institut de Recherche sur la Catalyse et l'Environnement de Lyon, CNRS, Lyon1, 2 Avenue Albert Einstein, 69626 Villeurbanne, France  
E-mail: [nadine.essayem@ircelyon.uni-lyon1.fr](mailto:nadine.essayem@ircelyon.uni-lyon1.fr), [shashank.mishra@ircelyon.univ-lyon1.fr](mailto:shashank.mishra@ircelyon.univ-lyon1.fr).

[b] Dr B. Lebeau  
Université de Haute Alsace, CNRS, IS2M UMR 7361, F-68100 Mulhouse,

[c] Dr B. Lebeau  
Université de Strasbourg, F-67000 Strasbourg, France

**Abstract:** Fluorinated zirconia were prepared by anionic exchange between commercial zirconium oxo/hydroxide of high surface area and trifluoroacetic acid solutions. The new fluoride-based catalysts contained high amount of F with superficial Zr/F ratio of 0.9 and 1.2 after calcination at 300°C and 400°C, respectively, and retained high surface areas. The impact of F insertion on the catalyst's acid-base properties was studied by calorimetry of NH<sub>3</sub> and CO<sub>2</sub> adsorption and FTIR of pyridine adsorption. The insertion of F species was shown to inhibit the basicity of zirconia and to generate Brønsted acidity ascribed to the electron withdrawing of Fluorine. This is consistent with the selectivity changes observed in the gas phase isopropanol conversion leading to formation of propene at the expense of acetone over zirconia and selective aqueous phase dihydroxyacetone conversion into pyruvaldehyde with reduced formation of hexoses and Lactic acid upon F loading within zirconia framework. Fluorine atoms also made the catalyst's surface more hydrophobic.

## Introduction

As compared to metal oxide nanomaterials, the potential of metal fluorides and oxo/hydroxo fluorides in heterogeneous catalysis remains much less trapped, even though they present excellent advantages of stronger acidity strength [1] due to electron withdrawing properties of fluorine atom present in the coordination sphere of metal sites as well as tunable Lewis/Brønsted acid sites balance [2,3]. These metal (oxo/hydroxo) fluorides have been already used as efficient solid acid catalysts in different reactions such as metal-acid catalysts for n-heptane cracking or n-pentane hydroisomerization [1]. In contrast to earlier applications of halogenated metals such as AlCl<sub>3</sub> or SbF<sub>5</sub> in Friedel-Crafts reactions, where a stoichiometric amount of the halogenated salt was needed [3,4], these nano metal (oxo/hydroxo) fluorides could be used in catalytic amount if the material presents a sufficient high surface area and stability. Even though the synthesis of nanometric metal fluoride catalysts has gained some momentum in the last decade, mostly by non-aqueous fluorolytic sol-gel method [3], it is limited to few metals for which commercial metal alkoxides are available [5]. Moreover, these syntheses use HF, which is a high-risk reagent.

This study proposes to design new fluorinated heterogeneous catalysts by anionic exchange between trifluoroacetic acid (TFAH) and zirconium oxo/hydroxide (ZrO<sub>x</sub>(OH)<sub>y</sub>), which would avoid using dangerous HF and highly moisture-sensitive and costly metal alkoxides. Although mildly corrosive in nature, trifluoroacetic acid does not pose the hazards associated with hydrofluoric acid and is a low-cost reagent. The trifluoroacetate anion is not only exchanged easily with oxo or hydroxo groups but is also decomposed conveniently to afford M-F bonds [6]. To the best of our knowledge, this methodology has never been reported to get fluorinated heterogeneous catalysts, in particular fluorinated zirconia. A far-reaching aim of this study is to develop a new range of solid acid catalysts which are active and stable in various acid catalyzed reaction conditions, related to petrochemistry where gas phase transformations are dominant or related to renewable oxygenated substrates valorization, facing the challenge of the design of solid acids catalysts tolerant to water. The catalytic performances of the new fluorinated zirconia are investigated in two model reactions: isopropanol conversion in gas phase and dihydroxy acetone conversion in aqueous phase.

## Results and Discussion

*Catalysts synthesized by anionic exchanges:*

By expanding our previous work on the synthesis of sulphated or tungstated zirconia via anionic exchanges with sulfuric acid or tungstic acid solutions [7,8], we describe here anionic exchange reaction between zirconium oxo/hydroxide ( $ZrO_x(OH)_y$ ) and trifluoroacetic acid (TFAH) solutions to obtain fluorinated zirconia as heterogeneous acid catalysts. The stirring of commercial zirconium oxo/hydroxide of high specific surface area ( $S = 401 \text{ m}^2\cdot\text{g}^{-1}$ ) in TFAH solutions for 15 min, followed by filtration and drying at ambient temperature for 72 h afforded  $ZrO_x(OH)_y/\text{TFA}$ . Further calcination of this precursor catalysts in a muffle oven for 2h at  $300^\circ\text{C}$  or  $400^\circ\text{C}$  resulted in the fluorinated zirconia catalysts abbreviated here as  $ZrO_2\text{-F-300}$  and  $ZrO_2\text{-F-400}$ , respectively.

*Fluorinated zirconia characterizations:*

**TGA-DTA analyses** were first used to identify the modifications brought to the zirconium-based material upon exchanges with trifluoroacetic acid. Figure 1 shows the TGA-DTA curves of unexchanged  $ZrO_x(OH)_y$  and those after TFA exchange, named  $ZrO_x(OH)_y/\text{TFA}$ . The TGA curve of  $ZrO_x(OH)_y$  shows a the first weight loss (10%) at temperature lower than  $120^\circ\text{C}$  with a parallel endothermic phenomenon due to the loss of physisorbed water. The second step, a progressive weigh loss (12%) between  $120^\circ\text{C}$  and  $\sim 450^\circ\text{C}$ , can be attributed to water losses through dehydroxylation [8]. The exothermic peak observed at  $445^\circ\text{C}$  corresponds to the crystallization of monoclinic zirconia [8]. The TGA curve of the TFA-exchanged material shows a the first progressive weight loss up to  $250^\circ\text{C}$  ( $\sim 7\%$ ), which is accompanied by weak endothermal phenomena at  $\sim 100^\circ\text{C}$  and  $170^\circ\text{C}$ . A rapid and important weight loss of 15% occurs between  $250\text{-}300^\circ\text{C}$ , associated with an exothermic peak at  $291^\circ\text{C}$ . Between  $300^\circ\text{C}$  and  $600^\circ\text{C}$ , the TGA curve displays a plateau. In this temperature range, a weak exothermic peak is observed at around  $400^\circ\text{C}$  due to the crystallization of zirconia. Starting at  $650^\circ\text{C}$ , another rapid weight loss is recorded together with a broad endothermic phenomenon. To interpret the different phenomena occurring during the thermal treatment of  $ZrO_x(OH)_y/\text{TFA}$ , TGA coupled with mass spectrometry was also performed (Figure S1). This study reveals that the important weigh loss between  $200$  and  $300^\circ\text{C}$  occurs with the parallel release of different ions of  $m/e = 44$  ( $\text{CO}_2^+$ ),  $45$  ( $\text{C}_2\text{H}_5\text{O}^+$ ),  $69$  ( $\text{CF}_3^+$ ) and  $51$  ( $\text{HCF}_2^+$ ). While the ethoxy groups are probably originated from the ethanol used as a solvent during the synthesis, the fluorinated species and  $\text{CO}_2$  are certainly released due to the decomposition of the trifluoroacetate groups [9]. At temperature higher than  $650^\circ\text{C}$ , only the ions with  $m/e=44$  is detected which could be from the zirconia surface decarbonation.

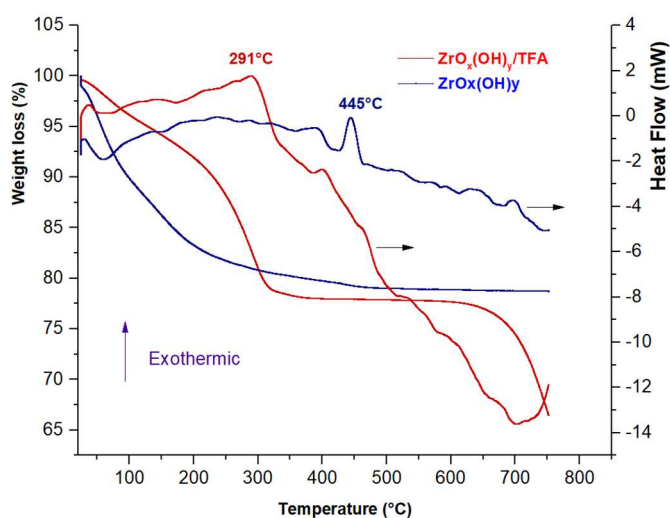


**Figure 1.** TGA-DTA curves of un-exchanged  $ZrO_x(OH)_y$  and  $ZrO_x(OH)_y/\text{TFA}$ .

$^{19}\text{F}$  MAS-NMR characterize the local environment of F at the atomic scale. Our first objective was to check if the synthesis procedure allows to retain F as trifluoroacetate groups (TFA) exchange with zirconium oxo/hydroxide  $ZrO_x(OH)_y$  in significant amount. The second objective was to get insights on the local environment of F as a function of the calcination temperature. Figure 2 compares the  $^{19}\text{F}$  MAS NMR spectra of as-synthesized  $ZrO_x(OH)_y/\text{TFA}$  to the materials obtained upon calcination at  $300^\circ\text{C}$  and  $400^\circ\text{C}$ , abbreviated as  $ZrO_2\text{-F-300}$  and  $ZrO_2\text{-F-400}$ , respectively.

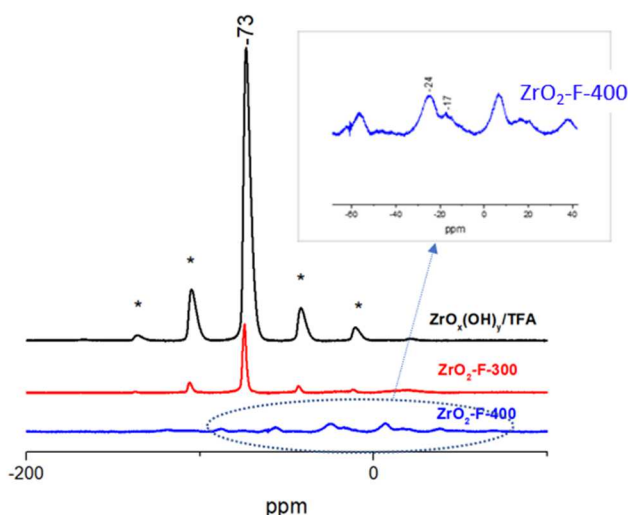


**Figure 2.**  $^{19}\text{F}$  MAS-NMR spectra of  $\text{ZrO}_x(\text{OH})_y/\text{TFA}$ ,  $\text{ZrO}_2\text{-F-300}$  and  $\text{ZrO}_2\text{-F-400}$  (\* represents spinning side bands).

$\text{ZrO}_x(\text{OH})_y/\text{TFA}$  exhibits a  $^{19}\text{F}$  MAS-NMR spectra with the most intense peaks at -73 ppm. Note that this resonance peak is dissymmetrical and may correspond to the resonance of two F species: 1) trifluoroacetate groups in exchange position on the surface of  $\text{ZrO}_x(\text{OH})_y$  and surface chelating or physisorbed TFA groups whose resonance peak is close to that recorded for trifluoroacetic acid at -74 ppm (Figure S2). Upon calcination at 300°C, the signal intensity is strongly reduced and become symmetrical at the chemical shift of 73 ppm. This lowering in signal's intensity may be due to a decrease of the F loading. Upon calcination at higher temperature of 400°C, the resonance peak at -73 ppm completely disappeared, and signals are detected at different chemical shifts at around -24 and -17 ppm. The disappearance of the thin resonance peak at -73 ppm is in agreement with the TGA curves which suggest the decomposition of the TFA group at temperatures higher than 200°C. The appearance of new resonance lines upon calcination for 2h at 400°C suggests that, as expected, F atoms are inserted within the zirconia matrix with the formation of Zr-F bonds.

**FTIR analyses** (Figure 3) confirm the presence of TFA groups in the catalyst. Indeed, the characteristic vibrations of trifluoroacetic acid (Figure S3) are observed in the spectrum of  $\text{ZrO}_x(\text{OH})_y/\text{TFA}$ . The stretching vibrations characteristic of TFA,  $\nu_{\text{as}}\text{COO}$  at 1670  $\text{cm}^{-1}$ ,  $\nu_{\text{s}}\text{COO}$  at 1450  $\text{cm}^{-1}$  and  $\nu_{\text{C-F}}$  at 1208  $\text{cm}^{-1}$  are present on the uncalcined  $\text{ZrO}_x(\text{OH})_y/\text{TFA}$  sample. After calcination at 300°C, these vibrations are still observable, but after calcination at 400°C, the vibrations due to trifluoroacetate groups disappeared, which is in good agreement with  $^{19}\text{F}$  MAS-NMR result.

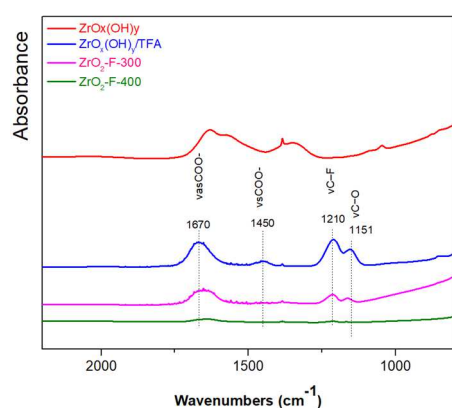


**Figure 3.** FTIR spectra of un calcined and calcined  $\text{ZrO}_x(\text{OH})_y/\text{TFA}$ .

**XRD analyses** of the fluorinated and non-fluorinated zirconia as a function of the calcination temperature are displayed in Figure 4. Till 300°C, the zirconia samples are amorphous, with or without Fluorine. After calcination at higher temperature, the F-free sample shows diffraction peaks corresponding to monoclinic and tetragonal zirconia (with the peaks indexing well with the JCPDS file 00-065-0728 of pure monoclinic  $\text{ZrO}_2$  phase and/or the JCPDS file 79-1765 of pure tetragonal  $\text{ZrO}_2$  phase). Upon F-doping, after calcination at 400°C, sharp diffraction peaks are observed, ascribed exclusively to monoclinic zirconia. One can underline that the stabilization of the monoclinic zirconia phase is contrary to the impact of doping zirconia with oxoanions such as sulfates, tungstates, molybdates, etc., known to favour the crystallisation of the tetragonal zirconia phase [7, 10]. The F-containing sample calcined at 400°C appears better crystallized than the non-fluorinated sample, most probably due to the formation of large crystalline domains of monoclinic zirconia phase. This is consistent with its lower specific surface area of 87  $\text{m}^2\cdot\text{g}^{-1}$ , while the F-free zirconia calcined at 400°C exhibits a specific surface of 226  $\text{m}^2\cdot\text{g}^{-1}$  (Table 1). As expected, the samples calcined at 300°C present higher surface areas: 213 and 328  $\text{m}^2\cdot\text{g}^{-1}$  for the samples  $\text{ZrO}_2\text{-F-300}$  and  $\text{ZrO}_2\text{-300}$ , respectively.

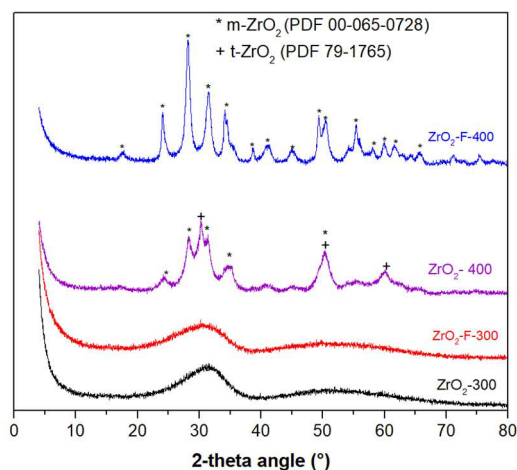


**Figure 4.** XRD patterns of ZrO<sub>2</sub>-F-300 and ZrO<sub>2</sub>-F-400. Comparison with F free samples: ZrO<sub>x</sub>(OH)<sub>y</sub> calcined at 300°C and 400°C: ZrO<sub>2</sub>-300 and ZrO<sub>2</sub>-400.

The nitrogen adsorption-desorption isotherms of the zirconia samples calcined at 300°C present hysteresis loops for relative pressure of 0.4 – 0.6, due to mesopores with diameter of 2–4 nm (Figure 5). These nitrogen isotherms also present also a significant uptake at low relative pressure, which is indicative of the presence of micropores. Their diameters are in the range of 1.2–1.6 nm (Table 1). The nitrogen adsorption-desorption of the fluorinated zirconia calcined at 400 °C does not present important N<sub>2</sub> uptake at low relative pressure and is characterized by a hysteresis loops at high relative pressure, >0.8.

**Table 1.** Textural properties of F-free ZrO<sub>2</sub> and F-doped ZrO<sub>2</sub> deduced from N<sub>2</sub> adsorption isotherms. Influence of the calcination temperature.

Samples <sup>[a]</sup>	S <sub>BET</sub> (m <sup>2</sup> .g <sup>-1</sup> )	S <sub>ext</sub> (m <sup>2</sup> .g <sup>-1</sup> ) <sup>[b]</sup>	∅ micro (nm) <sup>[b]</sup>	∅ meso (nm) <sup>[c]</sup>
ZrO <sub>2</sub> -300	328	34	1.2 -1.6	2-4
ZrO <sub>2</sub> -F-300	213	34	1.4 - 1.6	2-4
ZrO <sub>2</sub> -400	226	31	1.2 - 1.6	2-3.5
ZrO <sub>2</sub> -F-400	87	84	-	8-20

[a] Preliminary treated under vacuum at 300°C [b] Deduced from t-plot [c] Deduced from BJH method

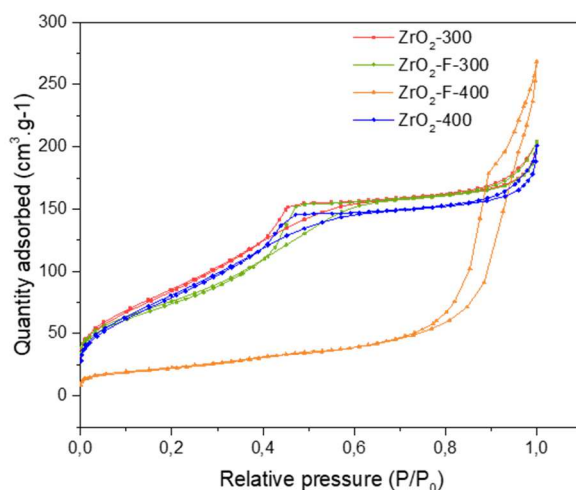


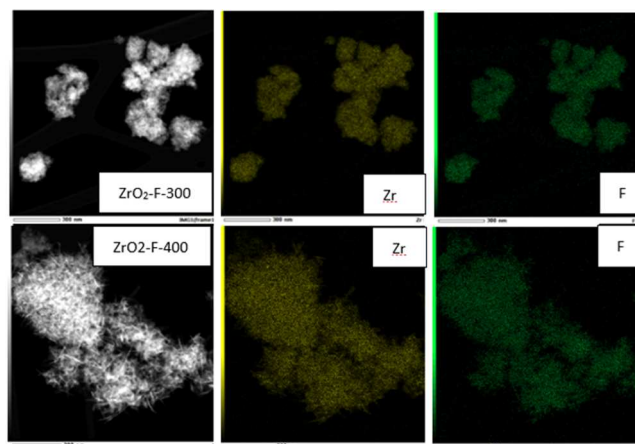
**Figure 5.** Nitrogen adsorption-desorption isotherms of fluorinated zirconia and of F-free zirconia calcined at 300°C and 400°C.

The TEM analyses reveal different morphologies of the fluorinated zirconia particles depending on the calcination temperature (Figure 6). Indeed, ZrO<sub>2</sub>-F-300 appeared as an amorphous material with spherical nanoparticles while ZrO<sub>2</sub>-F-400 presents many thin needles in line with the XRD data which showed sharp diffraction peaks of monoclinic zirconia phase. EDX analyses determined atomic Zr/F ratio of 3.2 for ZrO<sub>2</sub>-F-300. A significant lower F content was analyzed on ZrO<sub>2</sub>-F-400, with an atomic Zr/F ratio almost two time higher, between 5 and 6 (Table 2).

**Table 2.** Zr/F atomic ratio determined by EDX and XPS analyses.

	ZrO <sub>x</sub> (OH) <sub>y</sub> /TFA	ZrO <sub>2</sub> -F-300	ZrO <sub>2</sub> -F-400	Aged ZrO <sub>2</sub> -F-300	
				IPA test	DHA test
EDX	-	3.2	5 – 6.3	-	-
XPS	0.9	0.9	1.3	0.9	1.17

Zr and F elemental mappings disclosed the homogeneous fluorine dispersion within the ZrO<sub>2</sub> matrix regardless of the calcination temperature. This demonstrates that this anionic exchange synthetic method is an easy and safe way to introduce quite high fluorine loading, dispersed homogeneously within the ZrO<sub>2</sub> support.

**Figure 6.** TEM-EDX mapping of Zr and F elements within ZrO<sub>2</sub>-F-300 and ZrO<sub>2</sub>-F-400.

The XPS analyses of the uncalcined TFA-exchanged samples ZrO<sub>x</sub>(OH)<sub>y</sub>/TFA and those calcined ones, i.e. ZrO<sub>2</sub>-F-300 and ZrO<sub>2</sub>-F-400, gave further insights on the nature of F species together with their content and location.

From the XPS quantitative composition analysis of the sample's surfaces, it was evidenced that fluorine was preferentially on the zirconia surface, not only after the anionic exchange but also after the calcination steps (Figure S4). The values of the  $Zr_{total}/F_{total}$  atomic ratios obtained by XPS are significantly lower than the ones determined by EDX, which is a bulk analysis (Table 2). The  $Zr_{total}/F_{total}$  atomic ratio of the bulk is between 3.2 and 5-6, while by the XPS superficial analyses, the  $Zr_{total}/F_{total}$  ratio is 0.9 for the uncalcined sample and ZrO<sub>2</sub>-F-300, and 1.3 for ZrO<sub>2</sub>-F-400. These values also indicate the reduction of the F content upon calcination at higher temperature, which is consistent with <sup>19</sup>F MAS-NMR analysis. This could result from the changes in the structural and textural features upon calcination at 400°C.

The F 1s, O 1s and C 1s XPS peaks of the three samples are presented in Figure 7.

The F 1s XPS peak is evolving with the calcination: ZrO<sub>x</sub>(OH)<sub>y</sub>/TFA presents two distinct F 1s photoemission peaks at 688 and at 684 eV. With the calcination at 300°C, the relative intensity of the peak at higher binding energy, i.e. 688.3 eV, decreases significantly; at 400°C, only the peaks at lower binding energy, 685.7 eV remains. The peak at 688.3 eV was previously ascribed to chemisorbed CF<sub>3</sub> groups of TFAH [10,11]. The peak at around 685 eV, which corresponds of electron enrichment on the fluorine atom, could be attributed to F atoms incorporated within the zirconia matrix in the form of F-Zr bonds. The XPS O1s peak shows a similar evolution with the calcination temperature. On the uncalcined sample, two O1s photoemission peaks are observed at 530.3 eV, ascribed to the oxygen atom of zirconia framework [12], and at 532 eV due to the C-O and C=O bonds of TFA groups. Upon calcination, the relative intensity of the O1s peak ascribed to the TFA groups decrease progressively. The C1s spectrum also presents marked evolutions from the uncalcined sample to the ones calcined at the highest temperature. Four different C1s peaks are observed for ZrO<sub>x</sub>(OH)<sub>y</sub>/TFA. They are tentatively assigned as follows: the peak at the lowest binding energy, 284.8 eV is ascribed to aliphatic carbons, C-C, C-H, due to carbon contaminations. The two peaks at higher binding energies, 286 eV and 289 eV are attributed to the presence of ethoxy groups and the carboxylic groups, respectively [13,14]. The peak at 292.7 eV was previously ascribed to the carbon atom of the CF<sub>3</sub> group [10].

In agreement with the evolution of the XPS F1s and O1s peak, all the components due to the TFA groups progressively decrease with the calcination temperature, the peaks of contamination carbon at 284.8 becomes the main component after calcination at 400°C. These XPS analyses bring solid proofs in favor of F atom being incorporated within the zirconia surface upon calcination of TFA -exchanged zirconium oxo/hydroxide at a temperature as low as 300°C.

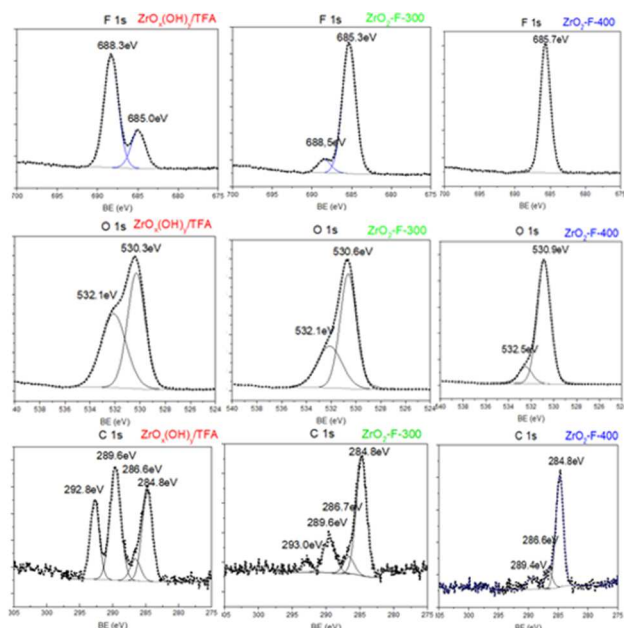


**Figure 7.** F 1s, O 1s and C 1s XPS peaks of  $ZrO_x(OH)_y/TFA$ ,  $ZrO_2-F-300$  and  $ZrO_2-F-400$ .

#### Characterization of the acid-base properties of fluorinated zirconia

Since zirconia is an amphoteric oxide, the F-free and F-incorporated catalysts were characterized both by calorimetry of  $CO_2$  and  $NH_3$  adsorption in gas phase. Figure 8 presents the calorimetric curves of  $NH_3$  adsorption and  $CO_2$  adsorption, i.e. the evolutions of the differential heat of adsorption with the surface coverage for the undoped and F-doped zirconia after calcination at 300 or 400°C. The corresponding isotherms curves are provided in Figure S5. The calorimetric curves of  $NH_3$  adsorption presents only few strong acid sites with heat of  $NH_3$  adsorption higher than  $120 kJ \cdot mol^{-1}$ , unrelated to the presence or absence of fluorine nor to the calcination temperature. One can conclude that the presence of fluorine did not rise the acid strength of the zirconium-based materials. For the fluorinated zirconia calcined at 300°C, there is indeed a contribution of the F addition on the acid sites density ( $\mu mole NH_3 \cdot m^{-2}$ ) and on the total amount of acid sites ( $\mu mole NH_3 \cdot g^{-1}$ ) easily deduced from the  $NH_3$  isotherms (Figure S5, Table 3). This solid is the most acid in the series with an acid site density of  $3.5 \mu mole \cdot m^{-2}$  and a total amount of acid sites reaching  $750 \mu mole \cdot g^{-1}$ . Moreover, the calorimetric curve of  $ZrO_2-F-300$  presents a pseudo plateau with a mean heat of  $NH_3$  adsorption at half coverage around  $110 kJ \cdot mol^{-1}$ . This indicates a rather homogenous surface in term of acid strength. By contrast, all the other samples are characterized by a continuous decrease of the heat of  $NH_3$  adsorption with the coverage which indicates the heterogeneity of their surface in terms of acid strength. Interestingly, the impact of F addition to the zirconia is more clearly highlighted by means of the calorimetry of  $CO_2$  adsorption which probes the surface basicity (Figure 8). It is observed that the two F-free zirconia, exhibit basic surfaces, with a base site density as high as  $1.3 \mu mole \cdot m^{-2}$  for the zirconia calcined at 400°C and  $0.5 \mu mole \cdot m^{-2}$  for the sample calcined at lower temperature. Note that the base strength of  $ZrO_2-400$  is the highest with initial heat of  $CO_2$  adsorption around  $110-120 kJ \cdot mol^{-1}$ . A remarkable result is the complete suppression of any basic sites after fluorine doping. The basic sites of zirconia were previously ascribed to the electronic charge density of  $O^{2-}$  ligands within the zirconia framework. The influence of F addition on the basicity might be explained by two phenomena: 1) the simple replacement of some superficial oxygen atoms by fluorine ones, the later ones would develop no basic character when entrapped in zirconia framework, and 2) the change of the electronic environment of the remaining superficial oxygen atoms as follows: the electron withdrawing properties of fluorine atom might decrease the electronic density on the oxygen atom, leading to the inhibition of their basic character.

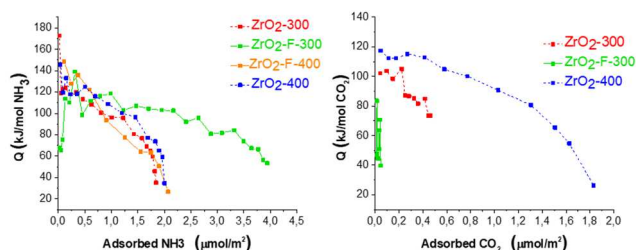


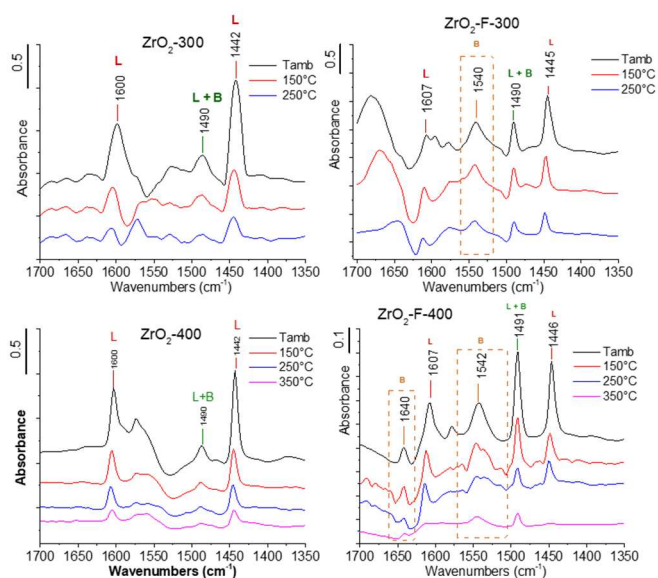
**Figure 8.** Calorimetry of  $NH_3$  and  $CO_2$  adsorption on F-free zirconia and fluorinated zirconia calcined at 300°C and 400°C. a-  $NH_3$ , b-  $CO_2$ .

**Table 3.** Acid and base properties of F-free zirconia and F-promoted zirconia deduced from calorimetry of NH<sub>3</sub> and CO<sub>2</sub> adsorption

Samples	Total <sup>[a]</sup> Acid sites μmole. g <sup>-1</sup>	Total <sup>[a]</sup> Basic sites μmole.g <sup>-1</sup>	S BET m <sup>2</sup> .g <sup>-1</sup>	Acid sites density μmole. m <sup>-2</sup>	Basic sites density μmole. m <sup>-2</sup>
ZrO <sub>2</sub> -300	500	100	328	1.5	0.5
ZrO <sub>2</sub> -F-300	750	~ 0	213	3.5	~ 0
ZrO <sub>2</sub> -400	370	300	226	1.6	1.3
ZrO <sub>2</sub> -F-400	120	~ 0	87	1.4	~ 0

[a] deduced from NH<sub>3</sub> or CO<sub>2</sub> isotherms (Figure S3)

To further understand the Fluorine impact on the zirconia acidity, FTIR studies of pyridine adsorption were undertaken. The spectra recorded on the different solids are gathered in Figure 9.

**Figure 9.** FTIR of pyridine adsorption on a) ZrO<sub>2</sub>-300 b) ZrO<sub>2</sub>-F-300 c) ZrO<sub>2</sub>-400 d) ZrO<sub>2</sub>-F-400

The bare zirconia, calcined at 300°C or 400°C, present only Lewis acid sites, characterized by the vibrations of the pyridine molecule coordinated to Lewis sites, at ~1442 and ~1600 cm<sup>-1</sup>. Both bands underwent similar decrease in intensity with the rise of the desorption temperature. This indicates that both samples have acid sites of similar acid strength, which is in good agreement with the calorimetry results. Upon Fluorine inclusion, irrespective of the calcination temperature, additional vibrations ascribed to the pyridinium species at 1540 cm<sup>-1</sup> are observed. In addition, the vibration at 1640 cm<sup>-1</sup> due to pyridinium species is also visible in the spectra of ZrO<sub>2</sub>-F-400. Similarly, the bands' intensity evolution with the rise of the temperature of desorption is very close for the two fluorinated zirconia. This suggests that upon F doping, Brønsted acid sites are generated and that the calcination temperature has no impact on their acid strength.

It is interesting to compare the acidity of this new fluorinated catalyst to some reference acid catalysts by mean of data drawn from calorimetric study of NH<sub>3</sub> adsorption done in similar conditions (Table 4). The total amounts of acid sites of ZrO<sub>2</sub>-F-300 is comparable to that of other acid oxides such as tungstated zirconia (ZrO<sub>2</sub>-W) or niobic acid (NbOH) but lower to that of zeolites (HY or HBeta with Si/Al=14), or of the sulfonated acidic resin Amberlyst-15 or the heteropolyacid, H<sub>3</sub>PW<sub>12</sub>O<sub>40</sub>. As regards to the acid strength of fluorinated zirconia, ZrO<sub>2</sub>-F-300 is the weakest solid acid within the series, with Q<sub>diff</sub> NH<sub>3</sub> of 110 kJ.mol<sup>-1</sup>, far below the strongest solid acid, H<sub>3</sub>PW<sub>12</sub>O<sub>40</sub> with Q<sub>diff</sub> NH<sub>3</sub> of 200kJ.mol<sup>-1</sup>.

**Table 4.** Acid properties of reference solid catalysts measured by calorimetry of NH<sub>3</sub> adsorption. Comparison with ZrO<sub>2</sub>-F-300

Samples	ZrO <sub>2</sub> -F-300 <sup>[c]</sup>	ZrO <sub>2</sub> -W [15]	Amberlyst-15 [16]	NbOH [17]	HY [17] Si/Al =14	HBeta [18] Si/Al =14	H <sub>3</sub> PW <sub>12</sub> O <sub>40</sub> [19]
Q <sub>diff</sub> NH <sub>3</sub> <sup>[a]</sup> (kJ.molNH <sub>3</sub> <sup>-1</sup> )	110	155	140	150	140	140	200
Acid sites amounts <sup>[b]</sup> (μmol.g <sup>-1</sup> )	500	350	2500	469	718	800	900

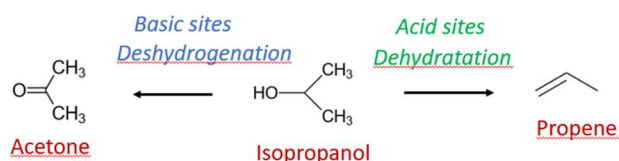
[a] Medium heat of NH<sub>3</sub> adsorption at half surface coverage [b] Q<sub>diff</sub> > 80 kJ.mol NH<sub>3</sub><sup>-1</sup> [c] present study

To rationalize above physico-chemical characterization of the fluorinated zirconia and their acid-base analysis, we propose that Fluorine atom, inserted preferentially within the surface of the zirconia framework, generates Brønsted acid sites, most likely in the form of acidic hydroxyl groups bonded to the superficial zirconium atom. In parallel, the electronic withdrawing effect of F atom would inhibit the basicity of the superficial O<sup>2-</sup> ligands as presented in scheme 1.

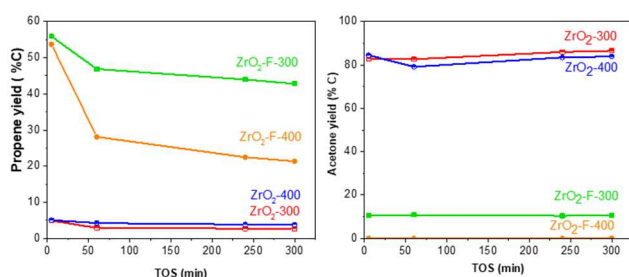
**Scheme 1.** Proposed structure of the acid and base sites of zirconia and fluorinated zirconia.

#### Fluorinated zirconia: insight on their catalytic properties

Two model reactions were used, one each in the gas and solution phase. The gas phase reaction was performed to evaluate the original acid base properties of the catalysts in absence of moisture. Gas phase isopropanol conversion was chosen owing to the reaction selectivity which depends on the acidity or basicity of the catalysts. The acid catalyzed pathway leads mainly to propene formation while the base catalyzed one leads to the formation of acetone (scheme 2).

**Scheme 2.** Model reaction of gas phase isopropanol conversion into propene catalysed by acid sites and into acetone catalysed by basic sites.

The yields in propene and acetone with time on stream are presented in Figure 10.

**Figure 10.** Isopropanol reaction over bare zirconia and F containing zirconia: a) Evolutions of propene yields b) Evolutions of acetone yields with time on stream.

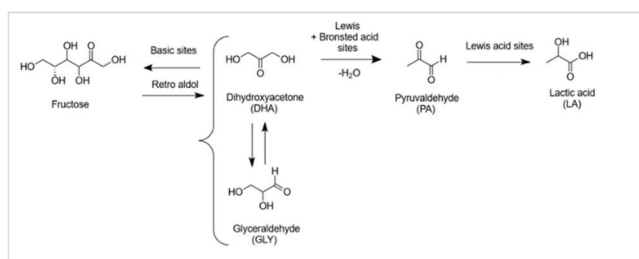
F-free zirconia, showed a significant and stable activity for isopropanol conversion into acetone irrespective of the calcination temperature, with acetone yields closed to 80%. The conversion of isopropanol into propene is not favoured over the two bare zirconia, the propene yields remain below 5%. The selectivity of the two bare zirconia for isopropanol conversion appears to be driven by their basicity. Their Lewis acidity would not intervene significantly for propene formation at least, the reaction being performed at relatively low temperature (250°C).

By contrast, F-containing zirconia showed a significant initial activity for isopropanol conversion into propene, with initial propene yield close to 55% for the two F-doped zirconia at the expense of acetone. Over ZrO<sub>2</sub>-F-400, acetone is not detected while a acetone yield reduced to 10% is obtained over ZrO<sub>2</sub>-F-300. Note that F-containing zirconia deactivated with time on stream. The

aged  $\text{ZrO}_2\text{-F-300}$  samples was recovered at the end of the reaction and analysed by XPS. The aged catalyst has still a Zr/F atomic ratio of 0.9, similar to that of the fresh catalyst (Table 2). This data indicates that its slight deactivation observed with time on stream was not due to loss of F-contents which would have caused a structural modification of the fluorinated zirconia. Accordingly, the XPS analysis of the aged catalyst (Fig. S6) does not show any modifications of the F1s XPS peak; its superficial carbon content remains in the same range of magnitude than the fresh catalyst, 7 at% against 10 at%.

To summarize, this first model reaction performed in gas phase has confirmed the inhibition of the zirconia basicity upon F loading. The Brønsted acidity generation caused by the F insertion would be at the origin of the catalysts' activity for propene formation from isopropanol dehydration. A similar high propene selectivity was reported over  $\text{H}_2\text{SO}_4$  treated zirconia-based catalysts [20].

To go further in the investigation of the catalytic potential of these new fluorinated zirconia catalysts, an aqueous phase model reaction capable of probing the water tolerance of acid sites as well as basic sites was chosen. Dihydroxyacetone (DHA) conversion in water appeared as the model reaction which fulfils our expectations. Indeed, we recently showed that the reaction selectivity depends not only of the Lewis/Brønsted acidity but also on the catalyst basicity: aqueous phase DHA conversion may produce pyruvaldehyde (PA) and Lactic acid (LA) catalysed by Brønsted/Lewis acid sites or hexoses (C6) catalysed by basic sites (Scheme 3) [21,22].



**Scheme 3.** Proposed parallel base and acid catalyzed DHA transformation pathways [13,14]

When comparing the activity of F-free zirconia to fluorinated zirconia, we first faced a surprising result: upon F doping the catalysts were less active than the bare zirconia (Figure 11). The initial rates of DHA conversion were roughly reduced by one order of magnitude without any apparent relation with the catalysts' specific surface areas, nor their original acid or base sites densities. Note that the DHA conversion over  $\text{ZrO}_2\text{-F-300}$  progressively increased with the time and reached a conversion of 55% at the reaction end, after 6h. This conversion remains lower than 73% and 65% conversion, achieved over  $\text{ZrO}_2\text{-300}$  and  $\text{ZrO}_2\text{-400}$ , respectively. On the other side, over  $\text{ZrO}_2\text{-F-400}$ , the DHA conversion increased only slightly with time up to 20% after 6h of reaction.

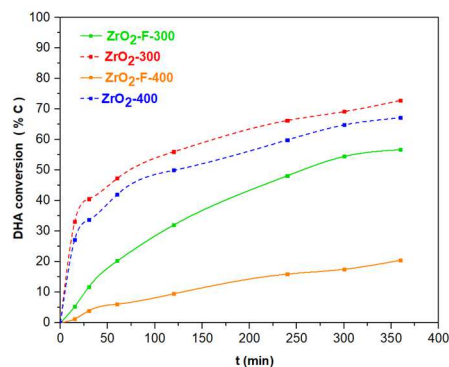


**Figure 11.** DHA conversion with time catalysed by F-free zirconia and fluorinated zirconia.

As expected, the salient results are the changes in selectivities upon F inclusion as shown in Figure 12.

Over bare zirconia calcined at 300°C or 400°C, hexoses and pyruvaldehyde are the main products with a behaviour of primary products in line with the pathway proposed in scheme 3. Hexoses formation is a base catalysed step from trioses aldolization. Pyruvaldehyde formation, at low temperature, can be promoted as well by Lewis or Brønsted acid sites. Only the formation of Lactic acid from pyruvaldehyde by rehydration requires Lewis acid sites. Lactic acid presents the behaviour of a secondary product formed from pyruvaldehyde over Lewis acid sites (Figure 12). These three products' yields are between 10 C% and 20 C% at the reaction end. One can conclude that the DHA reaction over bare zirconia is not selective and their acid-base surfaces appeared to be water tolerant.

Upon F insertion within the zirconia surface, the products selectivities changed strongly; the DHA conversion became more selective with pyruvaldehyde as main product. Its yield reached to 35 C% after 6h over  $\text{ZrO}_2\text{-F-300}$  while the Lactic acid and hexose reached to only 8 and 7 C%, respectively. The situation is quite similar for  $\text{ZrO}_2\text{-F-400}$  catalyst. The reaction became selective in pyruvaldehyde formation, with a yield close to 25 C%, while the yields of hexoses and Lactic acid remain lower than 3 C%. This change in selectivity is in good agreement with basicity inhibition upon F insertion, as deduced from the calorimetric analyses. The preferential formation of pyruvaldehyde over the fluorinated samples without significant further transformation into

Lactic acid may account for the generation of Brønsted acid site due to the fluorine. But this results indicate also that the original Lewis acid sites of the fluorinated zirconia might not be water tolerant contrary to our expectation.

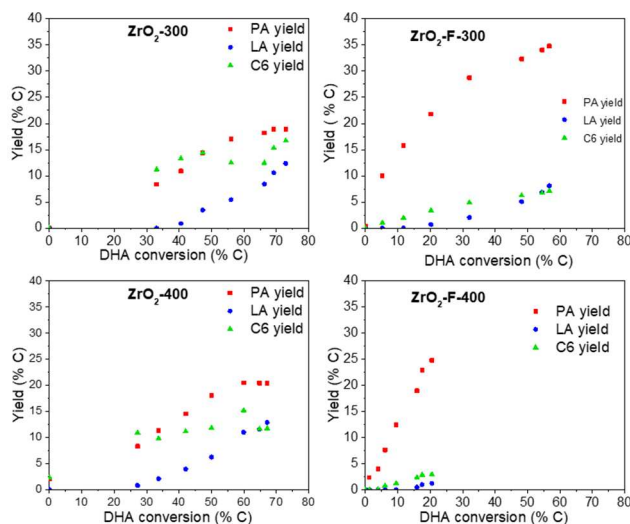


**Figure 12.** Evolutions of the products yields as a function of the DHA conversion over bare zirconia and Fluorinated zirconia.

At last, the overall reduced activity of fluorinated zirconia in water might be caused by its hydrophobic character simply due to the presence of fluorine. To check this hypothesis, isotherms of water adsorption were performed (Figure S7). The results indicate that indeed the F atom brings a hydrophobic character to the zirconia support. This can be viewed as a drawback for catalysis in water, but this can be tuned as an advantage since a more selective Brønsted acid surface is obtained by this way.

XPS analysis of the aged  $ZrO_2$ -F-300 catalysts recovered by filtration after the DHA reaction shows an increased atomic Zr/F ratio, from 0.9 for the fresh catalyst to 1.17 (Table 2). This indicates a slight F leaching in addition to an important amount of oxygenated organic compounds deposition leading to a total atomic % of carbon of 21% against 10% on the fresh catalyst (Figure S6).

## Conclusion

New metal oxo/hydroxo fluoride-based heterogeneous catalysts were successfully prepared by anionic exchange between a commercial oxo/hydroxo zirconium support of high surface area ( $ZrO_x(OH)_y$ ) and trifluoroacetic acid. The decomposition of the TFA groups in exchange position at the  $ZrO_x(OH)_x$  surface during calcination at 300°C and higher temperature results in the formation of F-species preferentially located within the zirconia surface with almost quantitative atomic ratio of Zr and F. The influence of Fluorine insertion on the superficial acid-base properties of zirconia was shown to inhibit the zirconia basicity and to generate Brønsted acid sites. The overall acid strength of F-containing zirconia is not changed as regards to bare zirconia. The impact of F on the suppression of the basicity and on the Brønsted acidity generation is consistent with the inductive electron withdrawing property of F, which is most probably present in the first coordination sphere of Zr. However, this effect does strengthen the Lewis acid strength of sites, assumed to be coordinatively unsaturated  $Zr^{4+}$  ion exposed at the surface.

The influence of F insertion on the acid-base properties of zirconia is confirmed by changes in the selectivities in two model reactions: gas phase isopropanol conversion and aqueous phase dihydroxyacetone conversion.

In gas phase, Fluorinated zirconia catalysed selectively the isopropanol dehydration into propene while non-fluorinated zirconia catalysed selectively isopropanol dehydrogenation into acetone. Although fluorinated zirconia is deactivated with time on stream, the XPS studies revealed that this is not due to the loss of fluorine content.

In aqueous phase, fluorinated zirconia became very selective into dihydroxyacetone dehydration into pyruvaldehyde without further rehydration into Lactic acid. Moreover, in agreement with the basicity inhibition, Dihydroxyacetone aldolization into hexose was suppressed. However, a slight F leaching was observed.

Finally, we attribute the reduced activity of the fluorinated zirconia in water as regards to non-fluorinated zirconia partly to the improved superficial hydrophobicity brought by the F atom. This was shown by isotherms of water adsorption at 20°C.

## Experimental Section

### Materials

Starting materials  $ZrO_x(OH)_y$  (MEL chemicals) and trifluoroacetic acid (Sigma Aldrich) were purchased from commercial sources (given in bracket) and used without further purification

### Synthesis of the fluorinated catalysts by anionic exchanges

5g of  $ZrO_x(OH)_y$  was dispersed in 75 mL of TFAH ( $CF_3COOH$ ) solution ( $1 \text{ mol.L}^{-1}$ ) and the suspension was stirred for 15 min and filtered. The recovered solid was first dried at ambient temperature for 72 h (abbreviated as  $ZrO_x(OH)_y/TFA$ ) and then calcined in a muffle oven for 2h at  $300^\circ\text{C}$  or  $400^\circ\text{C}$  using a heating rate of  $5^\circ\text{C.min}^{-1}$  to obtain fluorinated zirconia samples (abbreviated as  $ZrO_2-F-300$  and  $ZrO_2-F-400$ , respectively).

### General Procedures

The TGA/DTA data of the starting  $ZrO_x(OH)_y$  and TFA-exchanged  $ZrO_x(OH)_y$  were collected in air on a Setaram equipment with a thermal ramp of  $5^\circ\text{C/min}$

X-ray diffraction (XRD) measurements were performed on the powdered samples in a Bruker D8 Advance A25 diffractometer apparatus using  $\text{Cu K}\alpha$  radiation ( $0.154184 \text{ nm}$ ) at  $50 \text{ kV}$  and  $35 \text{ mA}$ . Powdered samples were analysed within a  $2\theta$  range of  $4-80^\circ$  at  $0.02^\circ$  per step and with an acquisition time of  $96 \text{ s}$  per step.

$^{19}\text{F}$  MAS-NMR spectra were recorded on a Bruker Advance III 500 WB spectrometer in a  $2.5 \text{ mm}$  triple H/X/Y probe with an applied rotation frequency of  $15-17 \text{ kHz}$ .

XPS characterization was performed on a Kratos Axis Ultra DLD spectrometer equipped with a hemispherical electron analyzer using monochromatic Al K- $\alpha$  X-ray radiation ( $1486.6 \text{ eV}$ ,  $12 \text{ mA}$ , and  $15 \text{ kV}$ ). Survey spectra were recorded with a Pass Energy of  $160 \text{ eV}$  and  $1 \text{ eV}$  step. High resolution spectra were recorded with a  $40 \text{ eV}$  Pass Energy and  $0.1 \text{ eV}$  step in the F1s, O1s, C1s and Zr3d regions. The binding energy of the C1s peak at  $284.8 \text{ eV}$  was taken as internal standard. The CasaXPS software version 2.3.25 was used to data treatment.

The textural properties were analysed via nitrogen physisorption at  $77\text{K}$  in a Micromeritics ASAP 2020 instrument. The catalysts were degassed at  $200^\circ\text{C}$  for 2 h under vacuum (heating rate  $5^\circ\text{C.min}^{-1}$ ). The BET method was used to determine the specific surface areas.

The water vapor adsorption/desorption isotherms were also determined by using a Micromeritics 3 Flex apparatus. A mass between  $180$  and  $300 \text{ mg}$  of solids were pretreated under vacuum at  $80^\circ\text{C}$  for 5 h. The quantity of sorbed water is expressed in  $\text{cm}^3$  of water per g of dehydrated sample

Transmission Electron Microscopy (TEM) observations were performed using a Jeol ARM-200F microscope working at  $200\text{kV}$ . Elemental mappings were done with an EDX Jeol Centurio detector.

Calorimetry of  $\text{NH}_3$  and  $\text{CO}_2$  adsorption was used to study the original acid-base properties of the solids. Experimental set up consist of TianCalvet calorimeter connected to a vacuum glass volumetric equipment to measure the differential heat of adsorption of the successive small amounts of the probe molecule up to the surface coverage and, in parallel, the isotherm of  $\text{NH}_3/\text{CO}_2$  adsorption. About  $50\text{mg}$  of sample was placed in a glass cell and further treated under vacuum at  $150^\circ\text{C}$  overnight. Subsequently, the glass cell, kept under vacuum, is placed into the calorimeter, and small doses of ammonia or carbon dioxide were introduced into the glass cell till the equilibrium pressure of the probe molecule was reached. The  $\text{CO}_2$  and the  $\text{NH}_3$  adsorptions were performed at  $30^\circ\text{C}$  or  $80^\circ\text{C}$  respectively using the same methodology.

Fourier Transformed Infrared (FTIR) spectroscopy of adsorbed pyridine were carried out to probe the nature of the acid sites. A Bruker Vector 22 FT-IR spectrophotometer equipped with DTGS detector was used. Self-supporting pellets ( $50 \text{ mg}$  of catalyst,  $18 \text{ mm}$  diameter) were used for pyridine adsorption studies. First, the pellet was vacuum treated at  $150^\circ\text{C}$ , then exposed to pyridine vapor pressure at room temperature for 5 min. The desorption was performed by outgassing the samples for 1 h at RT,  $150^\circ\text{C}$ ,  $250^\circ\text{C}$  and  $350^\circ\text{C}$  and the FTIR spectra of adsorbed pyridine were recorded at room temperature after each step. FTIR spectra were also obtained from solid catalysts samples diluted in KBr pellet (2%).

### Dihydroxyacetone (DHA) conversion in water

The reactions were conducted in a two-neck round bottom flask ( $25 \text{ ml}$ ) equipped with a water condenser, a temperature sensor and a rubber septum. At first, water and catalyst ( $10 \text{ g.L}^{-1}$ ) of a total volume of  $20 \text{ ml}$  were heated at  $90^\circ\text{C}$  in a controlled temperature oil bath and agitated by a magnetic stirrer. When the temperature stabilizes, DHA (Aldrich) powder was added ( $t=0$ ) and the reactions were conducted during 6 hours. The DHA initial concentration was  $0.1 \text{ mol.L}^{-1}$ . The reactant/products analysis was done using high-performance liquid chromatography (HPLC) (Model Shimadzu Prominence) with a refractive index detector (RID) equipped with a COROGEL 107H column, at  $40^\circ\text{C}$ , and acidified water ( $\text{H}_2\text{SO}_4$   $1.7 \text{ mM}$ ) was used as mobile phase ( $0.6 \text{ mL.min}^{-1}$ ).

### Conversion of propan-2-ol (Isopropanol) to propene and acetone

Gas-phase dehydration of isopropanol (IPA) was carried out in a flow-type reactor with a fixed catalyst bed at atmospheric pressure. The catalyst ( $80 \text{ mg}$ ) was introduced into a Pyrex glass tube reactor and pretreated under flowing nitrogen for 1 h at  $250^\circ\text{C}$  (heating rate  $5^\circ\text{C.min}^{-1}$ ). The catalytic reaction was carried out at the same temperature,  $250^\circ\text{C}$ , for 4 hours, using a total flow rate of  $10 \text{ L.h}^{-1}$  of IPA ( $5 \text{ Torr}$ ) diluted in nitrogen used as a carrier gas. The reaction products are analyzed on line by means of a GC-FID for IPA, propene, diisopropyl ether and acetone analysis.

## Acknowledgements

Roua Ben Salem thanks the French ministry of higher education, research and innovation for her PhD grant (doctoral school of chemistry, Lyon). Prof. Jean-Luc Blin (Univ. Lorraine, France) is sincerely thanked for fruitful discussions. We also thank Loïc Vidal in charge of the Electron Microscopy platform at IS2M for TEM/EDX analyses. Pascale Mascunan, Nicolas Bonnet, Yoann Aizac and Chantal Lorentz from the Ir@tech platform of IRCELYON, in charge of water isotherms, XRD and  $^{19}\text{F}$  MAS-NMR analyses are warmly acknowledged.

**Keywords:** fluorinated zirconia • anionic exchange • dihydroxyacetone conversion • isopropanol conversion • acid base catalysts

## References

- [1] A.. Corma, V. Fornes, *Appl. Catal.* **1990**, *61*, 175.
- [2] S.. Celerier, F.. Richard, *Catal. Comm.* **2015**, *67*, 26.
- [3] E. Kemnitz, *Catal. Sci. Technol.* **2015**, *5*, 786.
- [4] F. Frouri, S. Célérier, P. Ayrault, F. Richard, *Appl.Catal.B: Environmental* **2015**, *168-169*, 515.
- [5] C.P. Marshall, T. Braun, E. Kemnitz, *Catal. Sci. Technol.* **2018**, *8*, 3151A.
- [6] H. Ayadi, W. Fang, S. Mishra, E. Jeanneau, G. Ledoux, J. Zhang, S. Daniele, *RSC Adv.* **2015**, *5*, 100535-100545.
- [7] F. Figueras, J. Palomeque, S. Loridant, C. Feche, N. Essayem, G. Gelbard, *J. Catal.* **2004**, *226 (1)*, 25-31.
- [8] N. Essayem, V. Martin, A. Riondel, J.C. Vedrine, *Appl. Catal. A:General* **2007**, *326(1)*, 74-81.
- [9] S. Mishra, E. Jeanneau, A.-L. Bulin, G. Ledoux, B. Jouguet, D. Amans, A. Belsky, S. Daniele, C. Dujardin, *Dalton Trans.* **2013**, *42*, 12633–12643.
- [10] A. Dandach, B. Russbueltdt, J. Toufaily, A. Karout, T.Hamieh, N. Essayem, *Catalysis Letters* **2022**, <https://doi.org/10.1007/s10562-022-04037-9>
- [11] T. Giannakopoulou, N. Todorova, T. Vaimakis, S. Ladas, C. Trapalis, *J. Sol. Energy Eng.* **2008**, *130*,
- [12] B. Hamad, A. Perrard, F. Figueras, F. Rataboul, S. Prakash, N. Essayem, *J. Catal.* **2010** *269(1)*, 1-4.
- [13] F. Fusalba, D. Bélanger, *J. Phys. Chem. B* **1999** *103*, 9044–9054.
- [14] T.K. Kim, X.M. Yang, R.D. Peters, B.H. Sohn, P.F. Nealey, *J. Phys. Chem. B* **2000** *104*, 7403–7410.
- [15] A. Dandach, B. Russbueltdt, J.Toufaily, A.Karout, T.Hamieh, N. Essayem *Catalysis Letters*, 2022 <https://doi.org/10.1007/s10562-022-04037-9>
- [16] V.C.Nguyen, N.Q.Bui, P.Mascinan, T.T.H.Vu, P.Fongarland, N.Essayem *App. Catal. A, General* **2018** *552*, 184-191.
- [17] A.C. Doiseau, F.Rataboul, L.Burel, N.Essayem *Catal. Today* **2014** *226*, 176-184.
- [18] A.L.Mota Salinas, G.Sapaly, Y.Ben Taarit, J.C. Vedrine, N.Essayem *Appl. Catal. A:General* **2008**, *336*, 61-71.
- [19] B.Hamad, R.O.LopesdeSouza, G.Sapaly, M.G.Carneiro Rocha, P.G.Pries de Oliveira, W.A.Gonzales, E.Andrade Sales, N.Essayem *Catal. Com.* **2008** *10*, 92-97.
- [20] M.N. Goda, H.N. Abdelhamid, A.E.A.A. Said, *ACS Appl. Mater. Interfaces* **2020** *12*, 646-653.
- [21] I.Abdouli, F.Dappozze, M.Eternot, C.Guillard, N.Essayem *Molecules* **27** (2022) 8172.
- [22] A.B.S. Neto, A.C. Oliveira, S. Mishra, N. Essayem *Applied Catal. A: General* **2023**, *658*, 119165. <https://doi.org/10.1016/j.apcata.2023.119165>

## Supplementary Informations

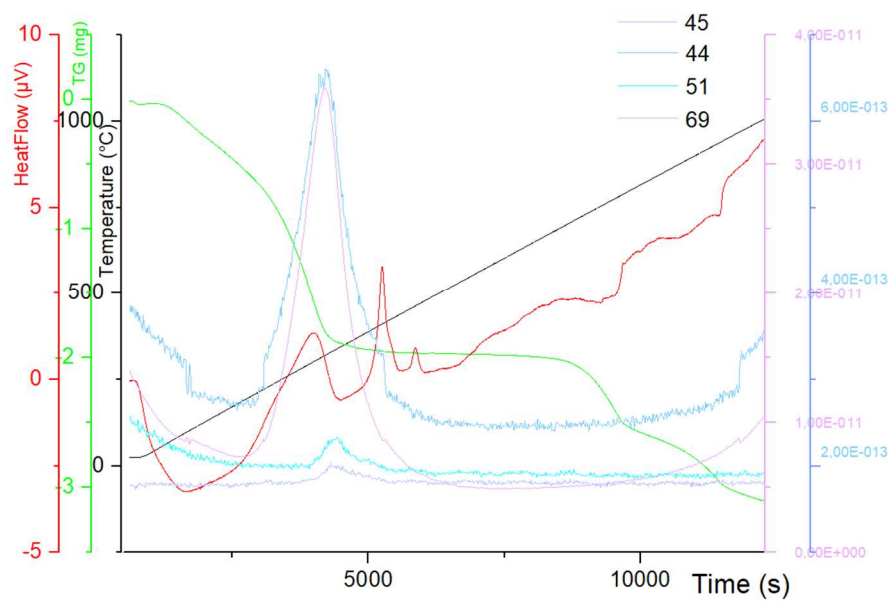


Figure S1 : SM analysis coupled to TGA-DTA analysis of ZrO<sub>x</sub>(OH)<sub>y</sub>/TFA

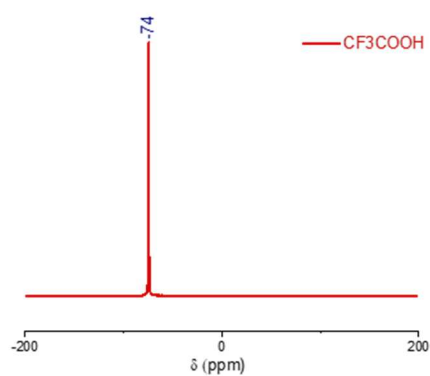


Figure S2 : Liquid <sup>19</sup>F NMR of Trifluoroacetic acid

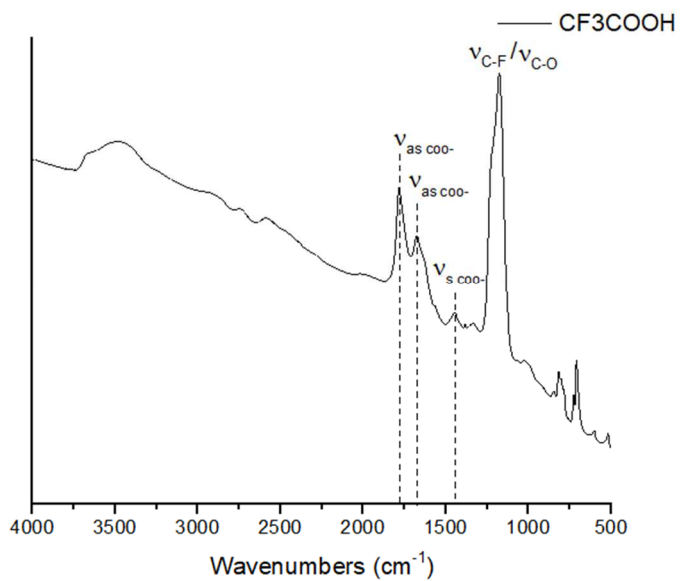


Figure S3 : FTIR spectrum of trifluoroacetic acid

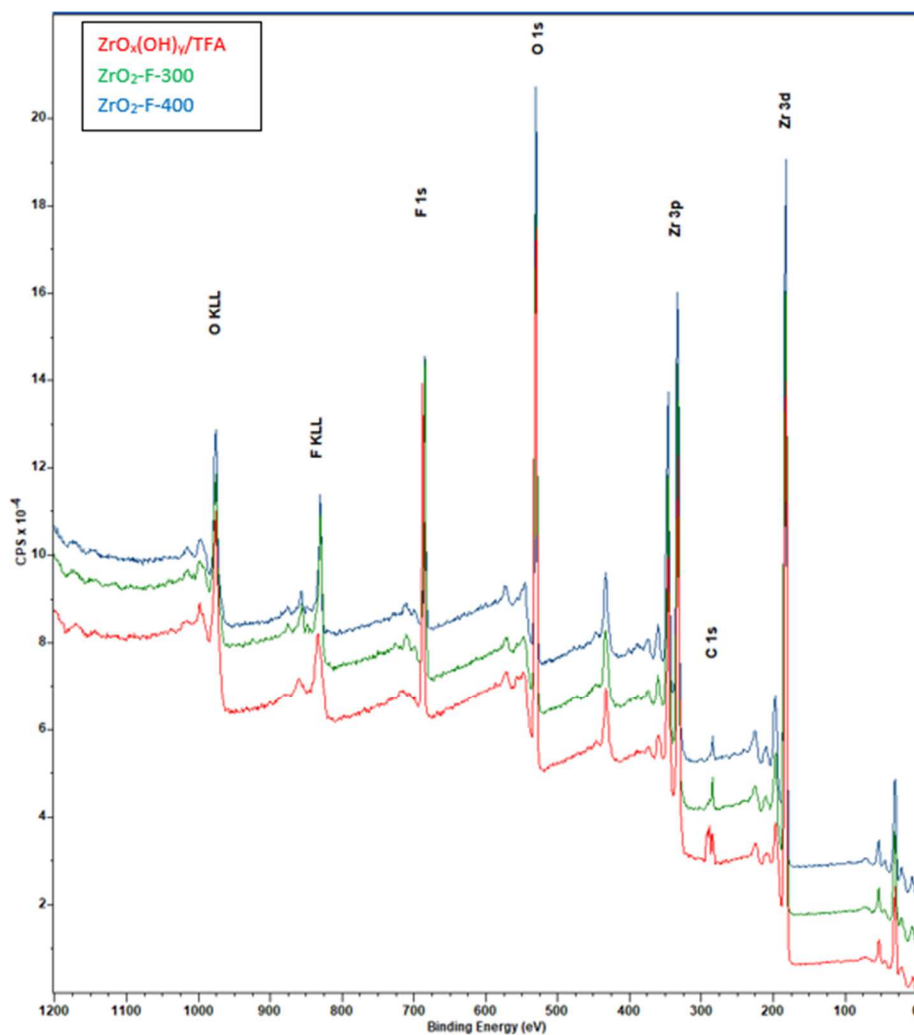


Figure S4: XPS survey spectra of fresh catalysts

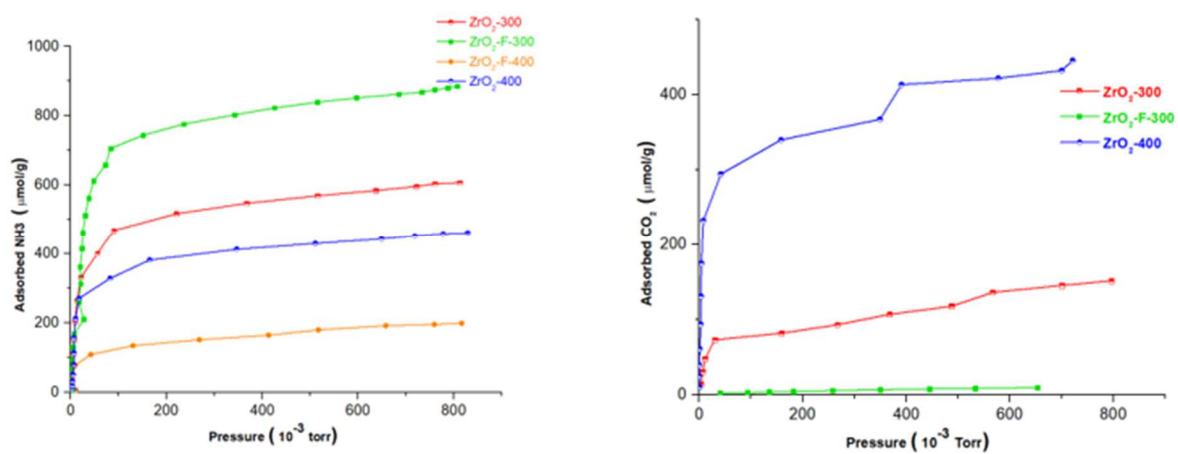
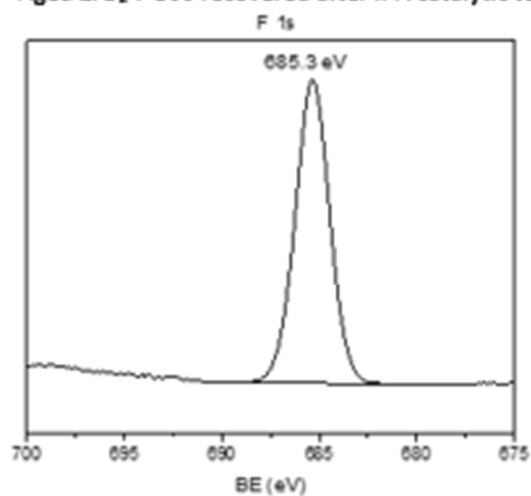


Figure S5 : Isotherms of NH<sub>3</sub> and CO<sub>2</sub> adsorption

Aged  $ZrO_2$ -F-300 recovered after IPA catalytic test



Aged  $ZrO_2$ -F-300 recovered after DHA catalytic test

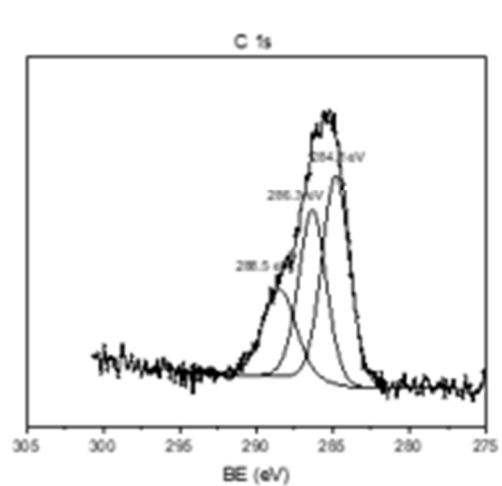
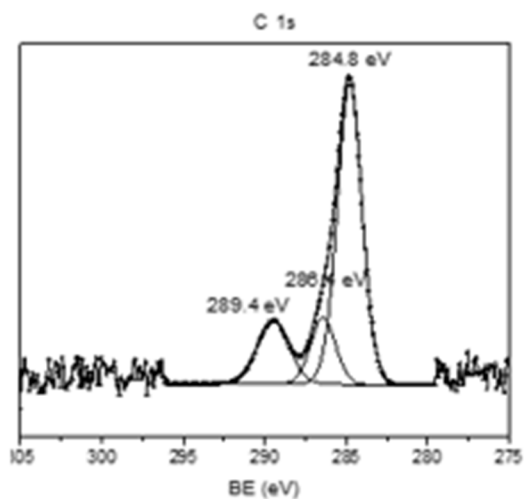
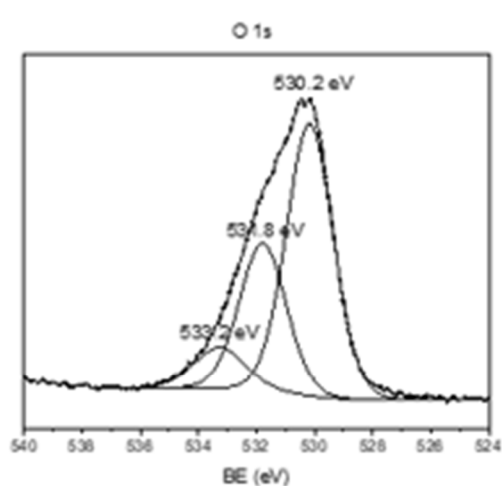
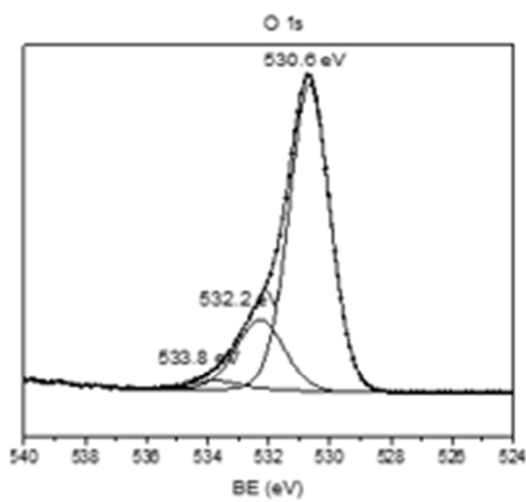
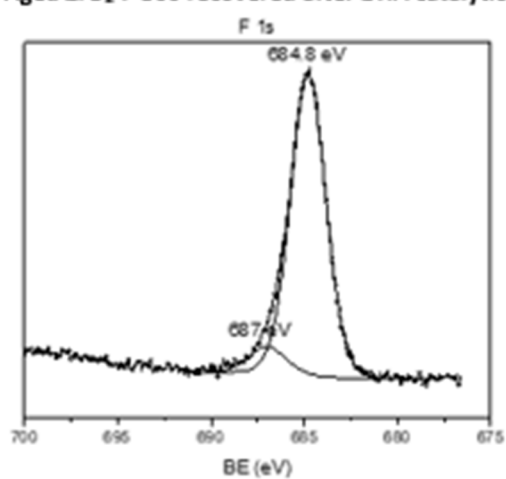


Figure S6: F 1s, O 1s and C 1s XPS peaks of aged  $ZrO_2$ -F-300 recovered after the reactions of liquid phase DHA conversion and gas phase IPA conversion.

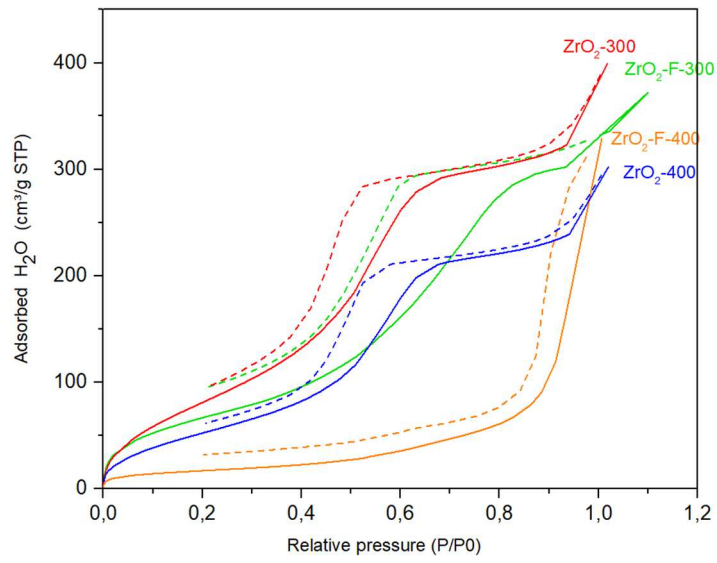


Figure S7 : Isotherms of water adsorption at 20°C over the zirconia samples: influence of F promoter and calcination temperature..